

## Level set approach to reversible epitaxial growth

M. Petersen,<sup>1,2</sup> C. Ratsch,<sup>2</sup> R. E. Caflisch,<sup>2</sup> and A. Zangwill<sup>1</sup>  
<sup>1</sup>*School of Physics, Georgia Institute of Technology, Atlanta, Georgia 30332*  
<sup>2</sup>*Department of Mathematics, UCLA, Los Angeles, California 90095-1555*

(Received 29 June 2001; published 26 November 2001)

We generalize the level set approach to model epitaxial growth to include thermal detachment of atoms from island edges. This means that islands do not always grow and island dissociation can occur. We make no assumptions about a critical nucleus. Excellent quantitative agreement is obtained with kinetic Monte Carlo simulations for island densities and island size distributions in the submonolayer regime.

DOI: 10.1103/PhysRevE.64.061602

PACS number(s): 81.15.Aa, 81.10.Aj, 81.10.Bk

### I. INTRODUCTION

At the present time, there is no practical approach to epitaxial growth modeling that bridges the gap between microscopic and macroscopic length scales. Rate equations offer some hope [1], but their reliance on uncontrolled mean-field approximations remains a serious obstacle. Kinetic Monte Carlo (KMC) simulations are very popular [2], but scale up to the micron range is very doubtful, even with future supercomputers.

One approach to the multiple-scale problem uses an atomic description in the vertical (growth) direction and a continuum description in the lateral directions. Specifically, the random walk of individual atoms on a flat terrace is replaced by the solution of a diffusion equation for the monomer density on each terrace. This is not a new idea [3], but its recent rebirth in the context of the *level set* (LVST) method [4–6] is particularly promising in light of the relatively low computational cost needed to treat arbitrarily complicated surface morphologies. So far, good success has been achieved for *irreversible* epitaxial growth where LVST calculations quantitatively reproduce the results of KMC calculations for the distribution of two-dimensional islands in the submonolayer regime [7].

The purpose of this paper is to extend the LVST method to the case of *reversible* epitaxial growth where thermal detachment of atoms from island edges is allowed. This step is necessary if one hopes to produce a model that is relevant to growth at elevated temperatures. Moreover, a reversible LVST growth model has significant computational advantages over a reversible KMC model. This is so because KMC keeps track of every detaching atom, including those that eventually return to the island from whence they came. Such events leave the system unchanged overall [8] and slow down the simulation significantly. By contrast, the reversible LVST scheme we develop below replaces these events by their time average and so includes only those detachments that do not lead to subsequent reattachments. Moreover, because of the mean-field approach, a large number of detachment events can be treated within a single simulation time step.

### II. METHOD

#### A. Level sets

The level set method [9] models the time evolution of arbitrarily shaped objects in  $n$  dimensions that can undergo

topological changes. In this paper, the relevant objects are two-dimensional islands and topological changes occur due to nucleation, dissociation, and coalescence. The key idea is to represent a curve or interface  $\Gamma$  in  $\mathbb{R}^n$  by the level  $k$  of a function  $\phi(\mathbf{x}, t)$

$$\Gamma_k = \{\mathbf{x}: \phi(\mathbf{x}, t) = k\}, \quad \mathbf{x} \in \mathbb{R}^n. \quad (1)$$

Here,  $\Gamma_k$  is the set of closed curves that constitute the perimeters of the islands with height  $(k+1)a$  ( $a$  is the lattice parameter).

Figure 1 illustrates the level set description of a typical epitaxial growth scenario. The left panel is a side view of two islands on a terrace (a) that grow to a pre-coalescence state (b) and subsequently merge (c). Later, a new island nucleates on top (d). The right panel shows the corresponding level set functions  $\phi$ . Note that it is not  $\phi$  that represents the surface morphology, but only the level sets ( $\phi=0$  and  $\phi=1$ ).

The motion of  $\Gamma$  is partly deterministic and partly stochastic. There is a deterministic part because a mean-field theory is sufficient to model the time average of many of the physical processes that contribute to growth. These effects

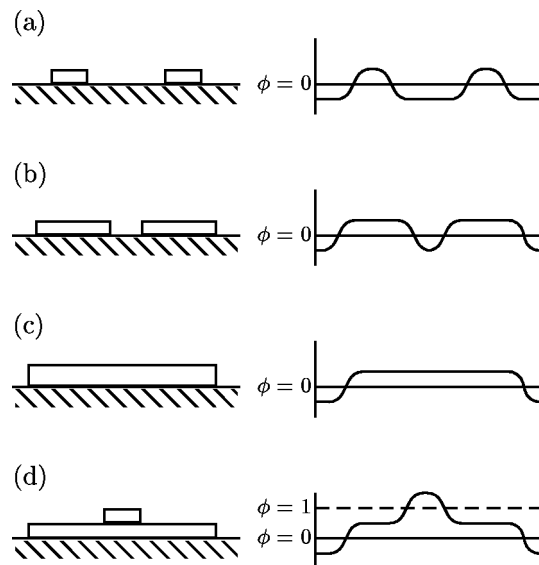


FIG. 1. Schematic illustration on mapping island configurations during growth (left panel) onto a LVST function  $\phi$ .

are built into a velocity function  $v_n(\mathbf{x}, t)$  that evolves the function  $\phi(\mathbf{x}, t)$  in time according to the partial differential equation

$$\dot{\phi}(\mathbf{x}, t) + v_n(\mathbf{x}, t) |\nabla \phi(\mathbf{x}, t)| = 0. \quad (2)$$

As the notation suggests,  $v_n$  is the component of the growth velocity in the direction of the local surface normal  $\mathbf{n} = \nabla \phi / |\nabla \phi|$ . The stochastic motion of  $\Gamma$  is associated with nucleation events and small-island dynamics. There is no unique algorithm to incorporate these effects into  $\dot{\phi}(\mathbf{x}, t)$ . The particular choice we make is explained in detail below.

### B. Deterministic evolution

It is convenient to write the velocity  $v_n$  in Eq. (2) in the form

$$v_n = v^{\text{att}} - v^{\text{det}}, \quad (3)$$

where  $v^{\text{att}}$  accounts for attachment processes that grow islands and  $v^{\text{det}}$  accounts for detachment processes that shrink islands. The first of these is proportional to the diffusive flux of atoms that approach an island edge from its bounding terraces. Therefore, if  $D$  is the surface diffusion constant and  $\rho(\mathbf{x}, t)$  is the adatom density, mass conservation gives

$$v^{\text{att}} = a^2 D \left( \frac{\partial \rho}{\partial n} \Big|_{\text{terrace}} - \frac{\partial \rho}{\partial n} \Big|_{\text{top of island}} \right). \quad (4)$$

We compute the required density from the mean-field, driven, diffusion equation

$$\dot{\rho}(\mathbf{x}, t) = D \nabla^2 \rho(\mathbf{x}, t) + F - 2 \frac{dN_{\text{nuc}}}{dt}. \quad (5)$$

The loss term in Eq. (5),

$$\frac{dN_{\text{nuc}}(t)}{dt} = D \sigma_1 \int_{\Omega} \rho(\mathbf{x}, t)^2 d^2x, \quad (6)$$

accounts for the dimers that nucleate as a result of binary collision between monomers. The total simulation area is  $\Omega$  and  $\sigma_1$  is the so-called ‘‘capture number’’ for an adatom [10]. We solve Eq. (5) subject to the boundary condition that  $\rho = 0$  at every point on  $\Gamma$ . This differs from the boundary condition usually used for reversible aggregation [11] because we have elected to incorporate all detachment effects into the velocity  $v^{\text{det}}$  (see Appendix A).

To find an explicit expression for  $v^{\text{det}}$ , we note first that most particles that detach from an island are driven back to that island by the diffusion field [11]. Our interest here is those particles that detach without subsequent reattachment, i.e., those that escape from the ‘‘capture zone’’ of the island. This is so because, by definition, the adatoms in the capture zone of a given island are guaranteed to attach to that island eventually. A relevant quantity is thus  $p_{\text{esc}}$ , the probability that a detached particle reaches the border of the capture

zone. The positions of these borders are easily calculated (the locus of points where  $\nabla \rho = 0$ ) and so is  $p_{\text{esc}}$ . We find (Appendix B) that

$$p_{\text{esc}} = \frac{\ln[(R_{\text{is}} + a)/R_{\text{is}}]}{\ln(R_{\text{cz}}/R_{\text{is}})}, \quad (7)$$

where  $R_{\text{is}}$  and  $R_{\text{cz}}$  are the radii of the circularly averaged island and capture zone.

We now define an effective escape rate per unit length of island perimeter as

$$R_{\text{det}} = D_{\text{det}} p_{\text{esc}} \lambda, \quad (8)$$

where  $D_{\text{det}}$  is an effective detachment rate and  $\lambda$  is the linear density of detaching particles (singly coordinated edge atoms). We use  $\lambda = 2$  for ‘‘small’’ islands and the expression [12]

$$\lambda = \frac{16}{3} \left( \frac{16}{15} v^{\text{att}} \frac{1}{D_{\text{edg}}} \right)^{2/3} \quad (9)$$

for ‘‘large’’ islands. The distinction between ‘‘large’’ and ‘‘small’’ islands will be made clear below.  $D_{\text{edg}}$  is the edge diffusion constant [13]. From  $R_{\text{det}}$  we get the desired expression for the detachment velocity that enters Eq. (3),

$$v^{\text{det}} = a^2 R_{\text{det}} = a^2 D_{\text{det}} p_{\text{esc}} \lambda. \quad (10)$$

Significantly (see below), there is negligible extra computational overhead needed to incorporate detachment in this way.

It remains only to find a home for the atoms that escape from the islands. In the spirit of the mean-field approximation, we return them to the adatom pool by simply augmenting the external flux. That is, the variable  $F$  in Eq. (5) is

$$F = F_0 + F_{\text{rev}}, \quad (11)$$

where  $F_0$  is the deposition flux and

$$F_{\text{rev}} = \frac{1}{\Omega} \int_{\Gamma} R_{\text{det}} d\Gamma \quad (12)$$

is the escape rate of atoms from all island edges. In this integral,  $\Gamma$  runs over all level sets of  $\phi(\mathbf{x}, t)$  [see Eq. (1)].

### C. Stochastic evolution

A nucleation event occurs when the variable  $N_{\text{nuc}}$  in Eq. (6) becomes larger than the next integer. This implies that  $\phi(\mathbf{x}, t)$  increases by a discrete amount at a discrete point. In the interest of numerical stability, we smooth out this increase over several points on the numerical grid used to solve Eq. (5). The exact position where the dimer nucleates is chosen randomly with the integrand of Eq. (6) as a weight factor [7].

Randomness is also important for detachment from ‘‘small’’ islands that consist of only a few atoms. Our approach is to choose an island area  $A_{\text{cut}}$  and treat all islands smaller than this size statistically. Thus, in a given time in-

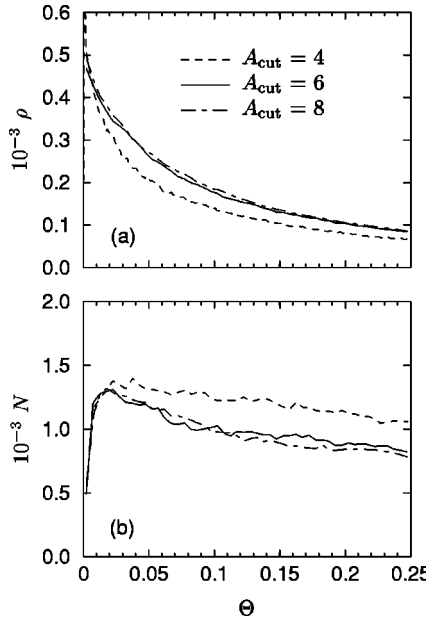


FIG. 2. Influence of  $A_{\text{cut}}$  on the adatom density  $\rho$  (a) and the island density  $N$  (b) as a function of coverage  $\Theta$  for  $D_{\text{det}}/D = 0.001$ . Data have been averaged over ten runs.

terval, we use Eq. (8) to calculate the total number of adatoms that detach from all islands smaller than  $A_{\text{cut}}$ . This corresponds to a total area loss  $A_{\text{loss}}$ . If  $A_{\text{loss}} > A_1$ , the area occupied by one atom, we detach an atom from one of the islands smaller than  $A_{\text{cut}}$ . The specific island that loses an atom is chosen randomly with  $p_{\text{esc}}$  as a weight factor. We then decrement  $A_{\text{loss}}$  by  $A_1$  and repeat the process until  $A_{\text{loss}} < A_1$ . This value is stored and added to the loss that occurs in the next time interval. If a detachment process leads to an island smaller than a dimer, we dissociate the dimer and decrement  $A_{\text{loss}}$  accordingly.

We emphasize that  $A_{\text{cut}}$  is *not* the area of a critical nucleus, i.e., an island that is absolutely stable against breakup. Instead,  $A_{\text{cut}}$  is merely the size of the smallest “large” island that we use as a parameter to switch between statistical and continuous detachment. In the context of our approach, the critical nucleus is defined by the condition  $v^{\text{att}} = v^{\text{det}}$  [see Eq. (3)].

### III. RESULTS

#### A. Parameter choices and systematics

All the LVST simulations reported here use the value  $D/F_0 = 10^6$ .  $D_{\text{edg}}$  in Eq. (9) was chosen as  $10^4$  and calculations were carried out on a  $200 \times 200$  lattice represented on a numerical grid of  $568 \times 568$  points. To determine  $A_{\text{cut}}$ , we compared runs with different choices for this parameter and looked for stabilization of the physical results. Thus, Fig. 2 compares island and adatom densities as a function of coverage  $\Theta$  obtained for  $A_{\text{cut}} = 4, 6$ , and  $8$  at a detachment rate of  $D_{\text{det}}/D = 0.001$ . Based on this data and related statistical tests, we find that our results are independent of  $A_{\text{cut}}$  if  $A_{\text{cut}} \geq 6$ . Therefore, we use  $A_{\text{cut}} = 6$  in all subsequent simulations.

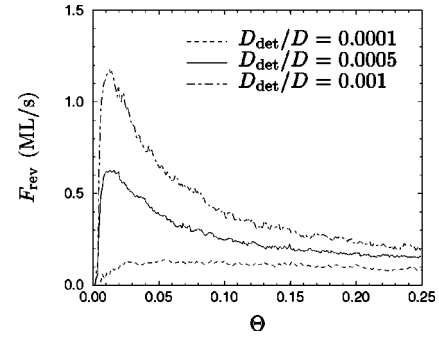


FIG. 3. Escape rate of atoms from all island edges  $F_{\text{rev}}$  [see Eq. (12)] as a function of coverage  $\Theta$  for different values of  $D_{\text{det}}/D$ . Simulation parameters as in Fig. 2, except  $A_{\text{cut}} = 6$ .

Figure 3 illustrates the role of detachment during growth. It shows  $F_{\text{rev}}$  from Eq. (11) as a function of  $F_0 t$  for different values of  $D_{\text{det}}/D$ . The fact that  $F_{\text{rev}}$  has its highest values at the earliest stages of growth (for the higher values of  $D_{\text{det}}/D$ ) shows that most of the effective detachment takes place when the islands are quite small. Indeed, as islands grow bigger, fewer particles escape from the island boundaries since the number of escaping particles relative to the perimeter of the growing islands becomes smaller and smaller.

#### B. Comparison to KMC

As a critical test, we compared our LVST results directly with KMC simulations [2,14]. In our KMC simulations adatoms are allowed to hop to a nearest-neighbor site at a rate  $r_n = D \exp(-nE_N/k_B T)$ , where  $n$  is the number of nearest neighbors,  $k_B$  the Boltzmann constant, and  $T$  the temperature. Adatoms are deposited at a rate  $F_0$ . In all simulations presented in this paper the ratio  $D/F_0$  is set to  $10^6$ . The energy barrier  $E_N$  is chosen such that  $D_{\text{det}} = D \exp(-E_N/k_B T)$ . In addition, singly coordinated edge atoms are allowed to diffuse along the step edge at a rate  $D_{\text{edg}}$ . We chose  $D_{\text{edg}} = D_{\text{det}}$ , but the results were not sensitive to this parameter as long as the islands were compact (as our LVST model assumes).

Figures 4, 5, and 6 respectively show the adatom density, island density, and island size distribution obtained by both methods as a function of detachment rate. These curves agree with previous reversible KMC simulations [11,15,16] that discuss, e.g., the physical origin of the observed saturation of the island densities and the sharpening of the island size distributions. Evidently, there is semiquantitative agreement between LVST and KMC. The size distributions results are particularly notable because they reflect information about spatial correlations that are averaged over to get  $\rho$  and  $N$ .

The only disagreement we find between LVST and KMC is for the saturation value of the island density for the smallest value of the detachment rate. We understand this based on recent research [17] with irreversible growth where a corresponding disagreement *vanishes* when the  $\rho = 0$  boundary condition for Eq. (5) is applied not at the true perimeter of each island (as we do) but instead at a closed boundary that exceeds the perimeter everywhere by one lattice constant. The disagreement disappears altogether when the island den-

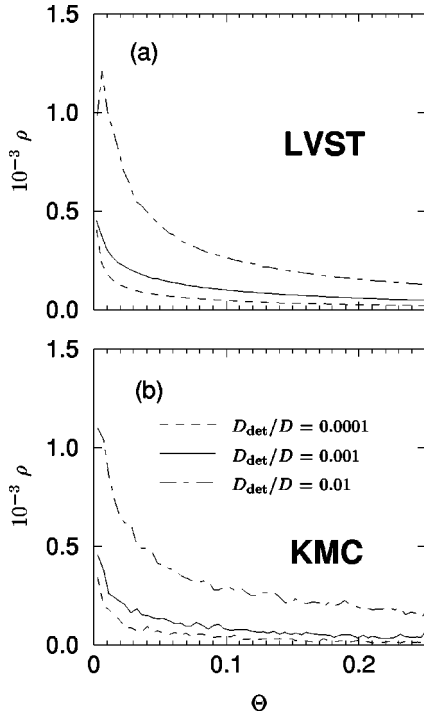


FIG. 4. Adatom densities as obtained by the level set method (a) and KMC (b). In the LVST calculation all parameters are as in Fig. 2, except  $A_{\text{cut}}=6$ .

sity is small. This is consistent with our observations because we get good agreement with KMC when the detachment rate is large (and the island density is small).

Figure 7 shows some systematic features of reversible growth as a function of the effective detachment rate. The

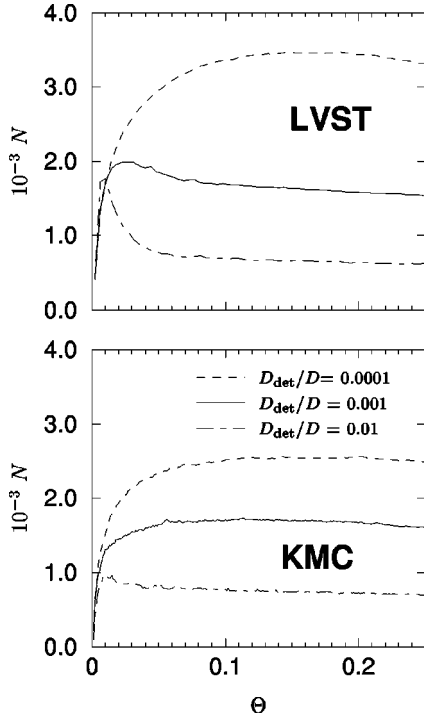


FIG. 5. Island densities  $N$  as obtained by the level set method (a) and KMC (b). Parameters as in Fig. 4.

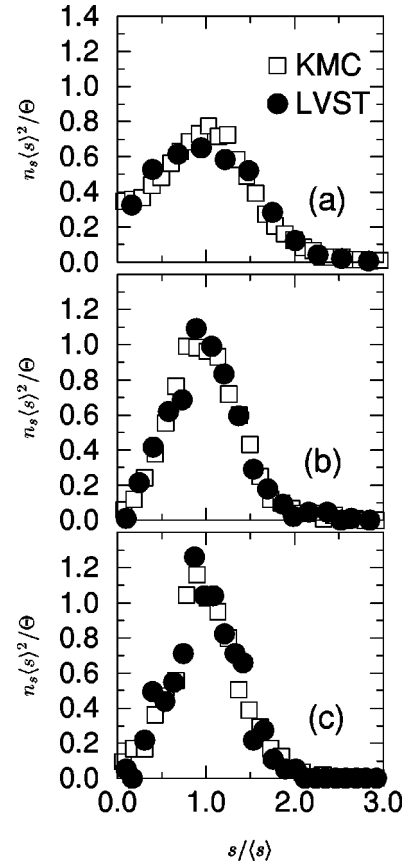


FIG. 6. Island size distributions where  $n_s$  is the density of islands of size  $s$ ,  $\langle s \rangle$  is the average island size, and  $\Theta$  is the coverage. Closed circles, level set result; open squares, KMC. Detachment rates are in (a),  $D_{\text{det}}/D=0.0001$ ; (b),  $D_{\text{det}}/D=0.0005$ ; and in (c),  $D_{\text{det}}/D=0.001$ . Data have been sampled at  $\Theta=0.25$ . Other parameters as in Fig. 4.

LVST data (collected at 0.25 ML coverage) show that the average adatom density increases linearly with  $D_{\text{det}}$  while the average island density decreases exponentially with  $D_{\text{det}}$ . Unfortunately, we have been unable to derive these interesting results analytically using rate equations.

The data in Fig. 6 was easy to obtain because, beginning with an irreversible growth simulation, the *extra* computational cost to include detachment is very small for LVST compared to KMC. This is so because LVST precisely suppresses the time-consuming detachment/attachment fluctuations that occupy a KMC simulation. Moreover, the LVST has essentially no restriction on the number of detachment events simulated during a specific time step. Quantitatively, Fig. 8 shows that the LVST method requires only negligibly more run time to include detachment whereas the KMC simulation cost increases sharply as the detachment rate increases. The LVST results depend very weakly on the rate of detachment because the increased cost is associated wholly with reductions in the step advance rate. Specifically, the adatom density rises with increasing detachment rate so the gradients evaluated in Eq. (4) become larger. But the step advance rate is limited by the condition that the boundary of the level set function can advance only one grid point in each simulation step. This implies that the scaling should be even

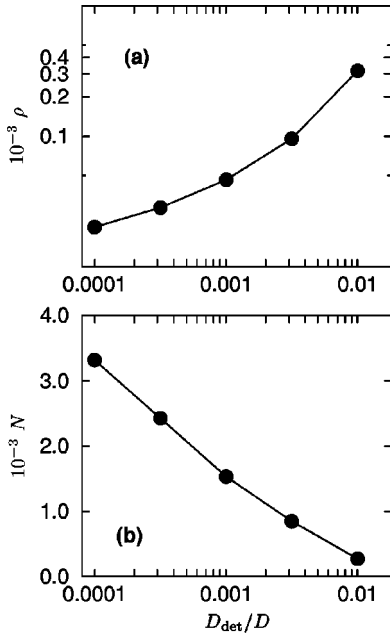


FIG. 7. Equilibrium adatom density  $\rho$  (a) and equilibrium density of islands  $N$  (b). Data have been sampled at 0.25 coverage. Other parameters as in Fig. 4.

better for simulations of, say, annealing processes, where there is no deposition flux and the adatom density is very low.

#### IV. CONCLUSION

In summary, we have developed a method to model epitaxial growth including atomic detachment from island edges within the context of the level set method. By all reasonable measures, the results are in excellent agreement with KMC simulations. Moreover, the LVST simulations scale significantly in CPU-time demand than KMC simulations when the effective detachment rate is large. This is so because our mean-field method eliminates the many atomic detachment events (each processed separately in KMC) that do not lead to successful escape from an island.

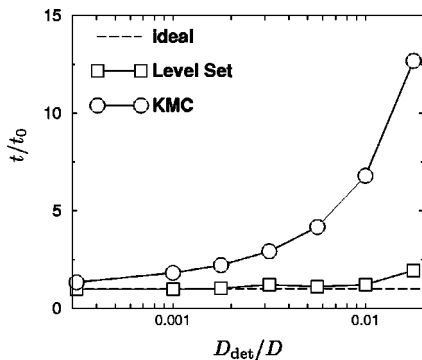


FIG. 8. Scaling of the level set and KMC method as a function of detachment rate. Runtimes  $t$  are normalized to the runtime of the irreversible case  $t_0$ . Parameters as in Fig. 4.

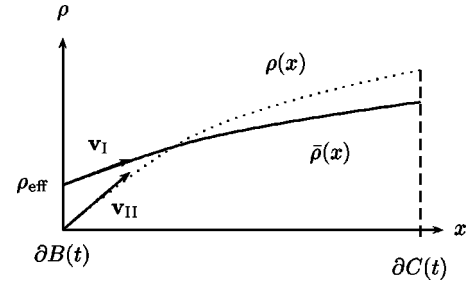


FIG. 9. Schematic illustration to the derivation of the equivalence of  $v^{\text{det}}$  and  $\rho_{\text{eq}}$ .

#### ACKNOWLEDGMENTS

We thank M. Kang, C. Andersen, S. Osher, and D. Vvedensky for helpful discussions. M.P. and A.Z. gratefully acknowledge the support of NSF DMR-953-1115. This work was also supported by DARPA through cooperative agreement DMS-9615854 as part of the Virtual Integrated Prototyping Initiative.

#### APPENDIX A: BOUNDARY CONDITIONS

The usual boundary condition for reversible growth [11] sets  $\rho = \rho_{\text{eq}}$  at every island perimeter. In this Appendix, we relate  $\rho_{\text{eq}}$  to the detachment velocity  $v^{\text{det}}$  used in this paper. The idea is to consider two adatom densities,  $\bar{\rho}$  and  $\rho$  as schematically shown in Fig. 9.  $\bar{\rho}$  ( $\rho$ ) is the system where the adatom density drops to  $\rho_{\text{eq}}$  ( $\rho = 0$ ) at the island boundary. We then write down diffusion for both adatom densities and derive from those the respective reversible growth velocities.

Let  $\bar{\rho}$  (the solid line in Fig. 9) be the exact solution of

$$0 = D\nabla^2 \bar{\rho}(\mathbf{x}) + F_0, \quad \mathbf{x} \in \Omega, \quad (\text{A1})$$

$$\bar{\rho}(\mathbf{x}) = \rho_{\text{eq}}, \quad \mathbf{x} \in \partial B(t), \quad (\text{A2})$$

where  $\Omega$  is the domain,  $\partial B(t)$  the island boundaries, and  $\rho_{\text{eq}}$  is the (finite) equilibrium value of  $\bar{\rho}(\mathbf{x})$  at the island boundaries due to detachment of atoms.

If  $C(t)$  is the capture zone and  $\partial C(t)$  its boundary (dashed line in Fig. 9), then with the boundary condition

$$\frac{\partial \bar{\rho}}{\partial n} = 0, \quad \mathbf{x} \in \partial C(t) \quad (\text{A3})$$

we can uniquely solve the diffusion equation (A1).

In this case the reversible growth velocity is given by Eq. (4) (labeled  $v_I$  in Fig. 9).

Now we want to replace  $\bar{\rho}$  by a adatom density  $\rho$  (dashed line in Fig. 9) such that

$$0 = D\nabla^2 \rho(\mathbf{x}) + F_0 + F_{\text{rev}}, \quad \mathbf{x} \in \Omega, \quad (\text{A4})$$

$$\rho(\mathbf{x}) = 0, \quad \mathbf{x} \in \partial B(t), \quad (\text{A5})$$

were  $F_{\text{rev}}$  is as explained in Eq. (11) the diffusive flux away from the island boundary due to detachment.

It follows from Eqs. (A1) and (A4) that

$$\nabla^2 \rho(\mathbf{x}) = \frac{F_0 + F_{\text{rev}}}{F_0} \nabla^2 \bar{\rho}(\mathbf{x}) \quad (\text{A6})$$

and therefore

$$\rho(\mathbf{x}) = \frac{F_0 + F_{\text{rev}}}{F_0} [\bar{\rho}(\mathbf{x}) - \rho_{\text{eq}}]. \quad (\text{A7})$$

If we want the two systems  $\bar{\rho}$  and  $\rho$  to be equivalent, then we must require

$$\int_{C(t)} \rho(\mathbf{x}) d^2x = \int_{C(t)} \bar{\rho}(\mathbf{x}) d^2x. \quad (\text{A8})$$

Combining Eqs. (A7) and (A8) we obtain

$$\frac{F_0 + F_{\text{rev}}}{F_0} \int_{C(t)} [\bar{\rho}(\mathbf{x}) - \rho_{\text{eq}}] d^2x = \int_{C(t)} \bar{\rho}(\mathbf{x}) d^2x, \quad (\text{A9})$$

which is equivalent to

$$F_{\text{rev}} \int_{C(t)} \bar{\rho}(\mathbf{x}) d^2x = (F_0 + F_{\text{rev}}) \int_{C(t)} \rho_{\text{eq}} d^2x. \quad (\text{A10})$$

If  $A(C)$  is the area of the capture zone, the relation between  $F_{\text{rev}}$  and  $\rho_{\text{eq}}$  is

$$F_{\text{rev}} = \frac{F_0}{\frac{1}{A(C)} \int_{C(t)} \frac{\bar{\rho}(\mathbf{x})}{\rho_{\text{eq}}} d^2x - 1}. \quad (\text{A11})$$

Assuming that  $R_{\text{det}}$  is independent of  $d\Gamma$  we can rewrite Eq. (12) as

$$F_{\text{rev}} = \frac{1}{\Omega} R_{\text{det}} L. \quad (\text{A12})$$

Then, Eq. (10) reduces to

$$v^{\text{det}} = a^2 \frac{\Omega}{L} F_{\text{rev}} = a^2 \frac{\Omega}{L} \frac{F_0}{\frac{1}{A(C)} \int_{C(t)} \frac{\bar{\rho}(\mathbf{x})}{\rho_{\text{eq}}} d^2x - 1}. \quad (\text{A13})$$

## APPENDIX B: DERIVATION OF $P_{\text{esc}}$

Any atom that detaches from an island but does not reach the capture zone boundary is driven by the diffusion field back to the island. In such a case,  $p_{\text{esc}}$  is zero. But if the detached adatom does reach the border of the capture zone,  $p_{\text{esc}}$  is 1. Therefore, to determine the probability distribution  $P(\mathbf{x})$  for all possible paths of a detaching adatom, we solve the diffusion equation

$$\nabla^2 P(\mathbf{x}) = 0, \quad (\text{B1})$$

with the boundary condition

$$P(\mathbf{x}) = \begin{cases} 0, & \mathbf{x} \in S_{\text{is}} \\ 1, & \mathbf{x} \in S_{\text{cz}} \end{cases}, \quad (\text{B2})$$

where  $S_{\text{is}}$  and  $S_{\text{cz}}$  are the border of the island and of the capture zone respectively. These boundary conditions represent the either successfully escape (probability 1 to reach  $S_{\text{cz}}$ ) or the reattachment to the island (0 at  $S_{\text{is}}$ ).

Equations (B1) and (B2) can in principle be solved for any island and capture zone geometry. But in our calculations we assume for simplicity a spherical average for both, the islands and the capture zones. For this case the general solution to Eqs. (B1) and (B2) is

$$P(\mathbf{x}) = \frac{\ln(|\mathbf{x}|/R_{\text{is}})}{\ln(R_{\text{cz}}/R_{\text{is}})}, \quad (\text{B3})$$

where  $R_{\text{is}}$  and  $R_{\text{cz}}$  are the radii of the island and of the capture zone. From this we obtain the escape probability of a detached atom by taking  $|\mathbf{x}| = R_{\text{is}} + a$  ( $a$  is the lattice parameter) because when an adatom detaches, it is roughly at distance  $a$  from the island boundary. Therefore,

$$p_{\text{esc}} = \frac{\ln[(R_{\text{is}} + a)/R_{\text{is}}]}{\ln(R_{\text{cz}}/R_{\text{is}})}. \quad (\text{B4})$$

- [1] H. M. Koduvely and A. Zangwill, Phys. Rev. B **60**, R2204 (1999); J. G. Amar, M. N. Popescu, and F. Family, Phys. Rev. Lett. **86**, 3092 (2001).  
 [2] S. Clarke and D. Vvedensky, J. Appl. Phys. **63**, 2272 (1988); H. Metiu, Y.-T. Lu, and Z. Y. Zhang, Science **255**, 1099 (1992).  
 [3] W. K. Burton, N. Cabrera, and F. C. Frank, Philos. Trans. R. Soc. London, Ser. A **243**, 299 (1951); S. Stoyanov and M. Michailov, Surf. Sci. **202**, 109 (1988).

- [4] R. E. Caflich, M. F. Gyure, B. Merriman, S. Osher, C. Ratsch, D. D. Vvedensky, and J. J. Zinck, Appl. Math. Lett. **12**, 13 (1999).  
 [5] S. Chen, M. Kang, B. Merriman, R. Caflich, C. Ratsch, R. Fedkiw, M. Gyure, and S. Osher, J. Comput. Phys. **167**, 475 (2001).  
 [6] D. L. Chopp, J. Comput. Phys. **162**, 104 (2000).  
 [7] C. Ratsch, M. Gyure, S. Chen, M. Kang, and D. Vvedensky,

- Phys. Rev. B **61**, R10598 (2000).
- [8] This is not strictly true since such detachment/reattachment processes can lead to overall diffusion of a two-dimensional island. We ignore this possibility in the present work.
- [9] S. Osher and J. A. Sethian, *J. Comput. Phys.* **79**, 12 (1988).
- [10] G. S. Bales and D. C. Chrzan, *Phys. Rev. B* **50**, 6057 (1994).
- [11] G. S. Bales and A. Zangwill, *Phys. Rev. B* **55**, R1973 (1997).
- [12] R. E. Caflisch, W. E. M. F. Gyure, B. Merriman, and C. Ratsch, *Phys. Rev. E* **59**, 6879 (1999).
- [13] Note that this gives a lower bound to  $\lambda$ , since Eq. (9) is derived assuming an infinite step and, therefore, corner atoms are explicitly excluded. Results in Ref. [12] are checked against KMC steady state.
- [14] R. S. Ross and M. F. Gyure, *Phys. Rev. B* **61**, 8602 (2000).
- [15] C. Ratsch, A. Zangwill, P. Smilauer, and D. D. Vvedensky, *Phys. Rev. Lett.* **72**, 3194 (1994).
- [16] C. Ratsch, P. Šmilauer, A. Zangwill, and D. D. Vvedensky, *Surf. Sci.* **329**, L599 (1995).
- [17] C. Ratsch, M. Kang, and R. E. Caflisch, *Phys. Rev. E* **64**, 020601 (2001).